Science Bulletin xxx (xxxx) xxx

Contents lists available at ScienceDirect

Science Bulletin

journal homepage: www.elsevier.com/locate/scib

Article

# Direct observation of atomic-level fractal structure in a metallic glass membrane

Hongyu Jiang [a,1], Jiyu Xu [a,1], Qinghua Zhang [a,b,f,*], Qian Yu [c], Laiquan Shen [a,b], Ming Liu [d], Yitao Sun [a], Chengrong Cao [e], Dong Su [a], Haiyang Bai [a,b,f], Sheng Meng [a,b,f], Baoan Sun [a,b,f,*], Lin Gu [a,b,f,*], Weihua Wang [a,b,f]

[a] Beijing National Laboratory for Condensed Matter Physics, Institute of Physics, Chinese Academy of Sciences, Beijing 100190, China
[b] Songshan Lake Materials Laboratory, Dongguan 523808, China
[c] Department of Materials Science & Engineering, Center of Electron Microscopy and State Key Laboratory of Silicon Materials, Zhejiang University, Hangzhou 310027, China
[d] Qian Xuesen Laboratory of Space Technology, Beijing 100094, China
[e] Department of Materials Science and Engineering, University of Wisconsin-Madison, Madison, Wisconsin 53706, USA
[f] School of Physical Sciences, University of Chinese Academy of Sciences, Beijing 100049, China

ARTICLE INFO

*Article history:*
Received 13 December 2020
Received in revised form 15 January 2021
Accepted 27 January 2021
Available online xxxx

*Keywords:*
Metallic glass
Atomic-resolution imaging
Fractal packing
Percolation theory

ABSTRACT

Determination and conceptualization of atomic structures of metallic glasses or amorphous alloys remain a grand challenge. Structural models proposed for bulk metallic glasses are still controversial owing to experimental difficulties in directly imaging the atom positions in three-dimensional structures. With the advanced atomic-resolution imaging, here we directly observed the atomic arrangements in atomically thin metallic glassy membranes obtained by vapor deposition. The atomic packing in the amorphous membrane is shown to have a fractal characteristic, with the fractal dimension depending on the atomic density. Locally, the atomic configuration for the metallic glass membrane is composed of many types of polygons with the bonding angles concentrated on 45°–55°. The fractal atomic structure is consistent with the analysis with percolation theory, and may account for the enhanced relaxation dynamics and the easiness of glass transition as reported for the thin metallic glassy films or glassy surface.



## 1. Introduction

The disordered atomic structure of metallic glasses (MGs) is crucial for understanding their superior and unique properties as well as the glass formation process [1–4]. However, determining the atomic structure of MGs has been a long-standing issue. Unlike crystalline alloys, the structure of MGs lacks the translational symmetry, rendering it difficult to be dissected with conventional diffraction methodologies [5]. Over the past sixty years, extensive theoretical and experimental efforts have been devoted to elucidating the structure of MGs, confirming the general existence of short-range order (SRO) and medium-range order (MRO). Many structural models were also proposed for the bulk MGs, including the "dense random packing", "solute-centered cluster" and "solute-centered quasi-equivalent cluster" models, etc. [6–10]. These models can describe the types of SRO motifs and the organization of the motifs in the MRO, yet generally break down at the length scales beyond MRO. Recently, the fractal packing model has also been introduced to describe the structure of MGs, based on the observed noncubic power laws correlating positions of the first peak of radial distribution function and the average atomic volume induced by compositional and pressure variations [11–14]. However, the ranges for the fractal scaling obtained from experiments are often limited within the length scale of MRO, and the fractal nature has been challenged by the heterogeneous nature of MG structure and non-affine atomic-scale deformation [15]. Obviously, testing the applicability of these structural models in real MGs relies on precisely resolving the positions of atoms in their long-range structure, which is almost impossible due to the complex 3D structural essence in bulk MGs.

Recently, the low-dimensional MGs have attracted much attention owing to their novel and unique properties inaccessible by their bulk counterparts. For example, the thin MG films or glassy surfaces are shown to display enhanced atomic dynamics several orders of magnitude larger than that of the bulk [16–18], and hence different glass transition and crystallization behavior [19,20]. Some low-dimensional MGs also exhibit much better electrochemical or mechanical properties than the bulk MGs [21,22]. Clearly, these properties are closely correlated with the unique

* Corresponding authors.
*E-mail addresses:* zqh@iphy.ac.cn (Q. Zhang), sunba@iphy.ac.cn (B. Sun), l.gu@iphy.ac.cn (L. Gu).
[1] These authors contributed equally to this work.

https://doi.org/10.1016/j.scib.2021.02.020
2095-9273/

structure of low-dimensional MGs. Further, the reduction in dimensionality also provides a possibility to directly image the atom positions in the structure of glassy materials with advanced electron microscopy techniques [23,24]. Here, we directly observed the atomic arrangements in atomically thin MG membranes with an advanced atomic-resolution imaging technique. The characteristics of the global and local atomic packing for the amorphous structure were determined. The formation mechanism for the amorphous fractal structure as well as its role in understanding the unique relaxation dynamics and glass transition in MG materials were also discussed.

## 2. Experimental

### 2.1. Sample preparation

The alloys with a nominal composition of $Zr_{70}Ni_{30}$ (at%) were prepared by arc-melting pure metals in Ti-getter high-purity argon atmosphere. The ion beam deposition (IBD) technique was used to fabricate the MG membranes. The nominal high cooling rate of the deposition process drives the glass transition in a similar manner as the conventional cooling method [25,26]. The deposition target with the size of ($100 \times 100 \times 2$ mm$^3$ was fabricated by copper-mold-casting. The electron transparent transmission electron microscopy (TEM) grids were used as the substrates (from TED PELLA, Inc.), which were covered with the supporting ultrathin carbon films with a thickness of 5 nm. Prior to the deposition of MG membranes, the substrates were heated to 473 K for 30 min in a vacuum chamber and the target was pre-sputtered for 300 s to remove the possibly existing volatile contaminants or oxide layer on the surface. The MG membranes were deposited via IBD in a high vacuum ($< 4 \times 10^{-4}$ Pa). Through tuning the deposition time (1–20 s), the MG membranes with different areal atomic densities were obtained at the same ion beam current of 20 mA and sputtering energy of 750 eV. The deposited MG membranes are preserved in the vacuum chamber before the scanning transmission electron microscopy (STEM) measurements).

### 2.2. STEM experiments and analysis

The aberration-corrected high-angle annular dark-field scanning transmission electron microscopy (AC HAADF-STEM) observations were conducted with a double spherical aberration-corrected high resolution scanning transmission electron microscope (JEM-ARM200F, with cold field-emission gun). The electron beam spot operated at 200 kV was less than 1 Å to realize the sub-angstrom resolution. Electrons scattered incoherently from the samples were recorded by the HAADF detector at a collection angle of 90–370 mrad and convergence angle 28 mrad. The images were recorded with an electron dose of $0.5 \times 10^6$ electrons nm$^{-2}$ s$^{-1}$ and an acquisition time was 8 s. StatSTEM software is used to refine the structures of HAADF-STEM images with a Gaussian model to further exclude the noise signals of substrates [27,28]. Then the thickness of MG membranes can be obtained by this software based on the scattered cross sections which increase monotonically with thickness. The areal atomic density of MG membranes is obtained with the total number of atoms from the StatSTEM software divided by the area.

### 2.3. Molecular dynamic simulations

Molecular dynamic (MD) simulations were performed with LAMMPS code [29]. The $Zr_{70}Ni_{30}$ MG was constructed with embedded atom method potential [30]. We used two model substrates to simulate fractal MG membranes. The first employ an external 9–3 potential imposed on metal atoms, $E = \varepsilon[\frac{2}{15}(\sigma^9/z^9) - (\sigma^3/z^3)]$, where $\varepsilon$ takes 1.0 eV, $\sigma$ takes 2.9 Å. The second uses a graphene sheet, where the LJ parameters are $\varepsilon_{\text{metal-C}}$ of 0.12 eV and $\sigma_{\text{metal-C}}$ of 2.62 Å. The two substrates give a similar adsorption energy of ~1 eV for metal atom, while the second gives the in-plane confinement of ~0.2 eV on graphene hollow sites. A ($200 \times 200 \times 30$) Å$^3$ box and a ($199.2 \times 200.2 \times 30$) Å$^3$ box are used for the two substrates respectively. Total metal atoms of from 800 to 5600 are considered corresponding to experimental deposition time and areal density. The temperature was controlled by the Nose-Hoover thermostat, and the time step is 1 fs. The simulated systems are pre-equilibrated at 10,000 K to achieve the gaseous state, and then the deposition process is driven with an external force of 0.5 eV Å$^{-1}$ applied on each atom at 300 K. Then the configurations obtained with 9–3 potential substrate are optimized to the local energy minima, while the configurations obtained with graphene substrate are further relaxed for 5 ns at 300 K.

## 3. Results and discussion

The atomically thin MG membranes are obtained by slowly depositing a $Zr_{70}Ni_{30}$ alloy target on an ultrathin carbon film above a copper grid via the IBD technique (Fig. S1a online). The AC-STEM imaging was shown to be a powerful technique to determine atom positions in crystalline materials [31,32]. In fact, this electron microscopy technique has also been recently employed to image the atom positions in free-standing monolayer amorphous carbon with the improvement of resolution [24]. Here, we use the HAADF-STEM to visualize the atomic positions of Zr and Ni in the MG membranes. The HAADF STEM mainly collects the inelastically scattered electrons from heavy elements by using a high-angle annular STEM detector (Fig. S1b online) [33]. Here, owing to the atomic number ($Z$)-contrast nature of the HAADF technique, the signals of heavy Zr and Ni atoms are much larger than those of light carbon and oxygen atoms from substrates, airborne organic molecules, and oxides. Consequently, the intra-layer atomic packing for the MG membranes can be explicitly resolved by the high-performance AC HAADF-STEM imaging. Fig. 1a–f display typical atomic-resolution HAADF-STEM images for the $Zr_{70}Ni_{30}$ membranes with different deposition times (4, 7, 10, 13, 16, and 20 s). The bright spots in the images represent the positions of metallic atoms. The disorder arrangement of metallic atoms in the long-range reflects the amorphous nature of the $Zr_{70}Ni_{30}$ MG. The amorphous nature of these membranes was also confirmed by the halo ring in the fast Fourier transform (FFT) pattern (Fig. 1g) and the convergence of radial distribution function (RDF) spectra in the long-range below. The similar amorphous structures were also obtained with the nonplanar carbon nanotube substrates which relax the residual stress (Fig. S2 online). Meanwhile, MG membranes of different areal densities can be obtained by varying the deposition time, and the areal atomic density is found to be roughly proportional to deposition time (Fig. 1h).

We can extract the thickness of the MG membranes by using the StatSTEM software [27]. To illustrate this, we choose two representative samples with the areal density of 3.2 and 11.3 nm$^{-2}$, respectively. As shown in the atom counting results (Fig. 2a, b), the thickness of both MG membranes is less than three-atom layers, and more importantly, the first layer at the bottom (blue atoms) contributes to the most area of the MG membrane, suggesting the two-dimensional (2D) growth model of the MG membranes. Fig. 2b shows that the distribution of atoms in the membrane is not homogenous, but exhibits complex branching patterns, which may indicate the fractal nature of the atomic structure. To reveal this, we perform a geometrical fractal analysis on the HAADF-STEM images with different areal densities. We first

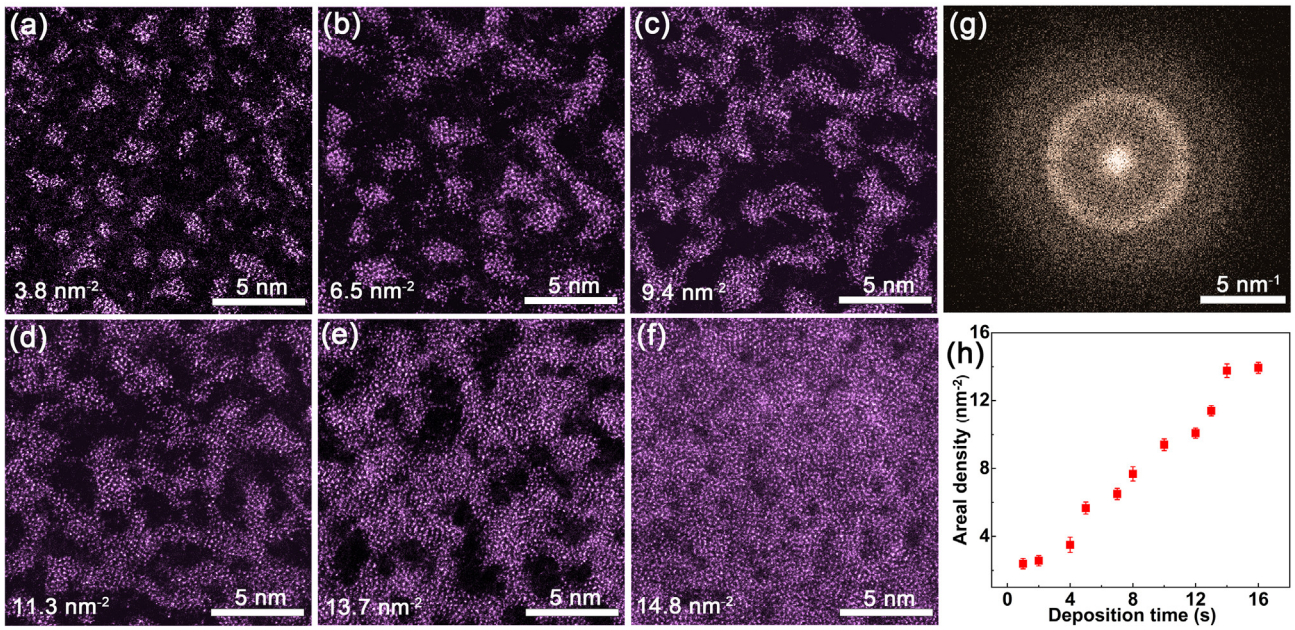


**Fig. 1.** (Color online) Disordered packing of MG membranes. (a–f) HAADF-STEM images of the $Zr_{70}Ni_{30}$ MG membranes with the different deposition times of 4, 7, 10, 13, 16, and 20 s. The corresponding areal density is marked in the lower-left corner of each image. (g) FFT pattern of the HAADF-STEM image in (e). (h) The plot of the areal atomic density versus the deposition time.

obtained the refined HAADF-STEM images of MG membranes with clear atomic positions with StatSTEM software (Fig. S3 online) [28]. Then we use the box-counting method to quantify these images, i.e., counting the number of boxes, $N(L)$, that could cover at least one atomic point in the image given the length of the box, $L$ [34]. Generally, $N(L)$ is correlated with $L$ by the formula $N(L) \sim L^{-D}$. If $D$ is a non-integral ($1 < D < 2$), the structure can be defined as a fractal and the exponent $D$ can be regarded as the fractal dimension. The typical plot of $N(L)$ versus $L$ for the MG membrane corresponding to Fig. 2b is shown in Fig. 2e. One can see that over a wide range of $L$, $N(L)$ can be well fitted by $N(L) \sim L^{-D}$ with $D = 1.63 \pm 0.01$, which indicates the fractal nature of the atomic packing [35]. While at the large end of $L$, $N(L) \sim L^{-2}$, corresponding to the recovery of 2D in the long-range. The fractal scaling breaks down at a length of ~20 Å, indicating the fractal structure can well extend in the long-range scale. This is different from that of bulk MGs where the observed fractal scaling is only limited within the MRO range [11–15]. The finite size of the fractal is counted with the percolation analysis below.

The fractal dimensions for MG membranes with different areal densities are also determined with the box-counting method (Fig. 2f). One can see that the fractal dimension shows a general increasing trend with the areal density, in the range of 1.2–1.8. At low areal density, the metallic atoms prefer to form elongated clusters (Fig. 2a). Statistical analysis showed that the average length-width ratio increases with the deposited areal density (Fig. S4 online), which leads to the contact of adjacent clusters and the formation of mesh patterns (Fig. 2b and Fig. S5c online). Further deposition enhances the compactness of the membranes and leads to the formation of individual voids on the surfaces (Fig. S5d online). The complete MG membrane can be obtained by filling the voids in the fractal structure via further deposition, where 2D recovers in the full range. We note that the complete MG membrane still exhibits the atomic thickness.

To reveal the underlying mechanism, we performed MD simulations of the MG membranes on model substrates. The simulation procedure follows the deposition experiments. After equilibrium at high temperatures to realize the gaseous state, the metallic atoms are driven to deposit onto the substrate with an external force of 0.5 eV Å$^{-1}$. Fig. 2c, d show the atomic packing for the simulated MG membranes on 9–3 potential substrate with the same areal density with Fig. 2a, b, respectively. It can be seen that these simulated MG membranes exhibit similar topological structures with those observed in STEM experiments. The fractal dimensions calculated for the simulated MG membranes are nearly the same as those of experimental membranes (Fig. 2f). All these evidences verify the fractal nature of the atomic structure in MG membranes.

Given the ideal and structureless 9–3 potential substrate, it is the delicate metallic interactions that dominate the emergence of fractal MG. The fractal is the distinctive character of metallic systems, and the depositions with other species give rise to the disappearance of fractal and the different configurations (Fig. S6 online). However, the stability of the fractal MG membrane relies on the balance between metal-metal interactions and metal-substrate interactions. The fractal structure is easy to coalesce and forms a large membrane structure on the wall substrates, while the fractal MG membrane is stable during the 5-ns-long MD simulation with the inclusion of realistic substrate lattice. Therefore, the formation of the fractal structure relies not only on the deposition process but also on an adequate balance of interactions between metal atoms and substrates [36]. The feasible substrates should exhibit a nice compatibility with metallic systems and adequate adsorption to confine the metallic atoms (Fig. S7 online) [25,37,38]. The schematic of the formation processes of the fractal MG membrane is shown in Fig. S8 (online). The ejected atoms undergo the quick transition from gaseous states to solid states, and the deposited structures are constrained to the metastable configurations via the balance of various interactions. The nominal cooling rate is ultrafast and gives rise to the hyper-quenched fractal MG membranes [25,26].

Besides the global atomic packing, we also analyzed the characteristics of the local atomic configuration. Fig. 3a–c shows the atomic images of three MG membranes with the areal densities of 2.8, 3.6, and 7.3 nm$^{-2}$, respectively. For analysis, the nearest neighbor atoms are connected with lines to form different types of polygons. A close examination of the images in Fig. 3a–c showed

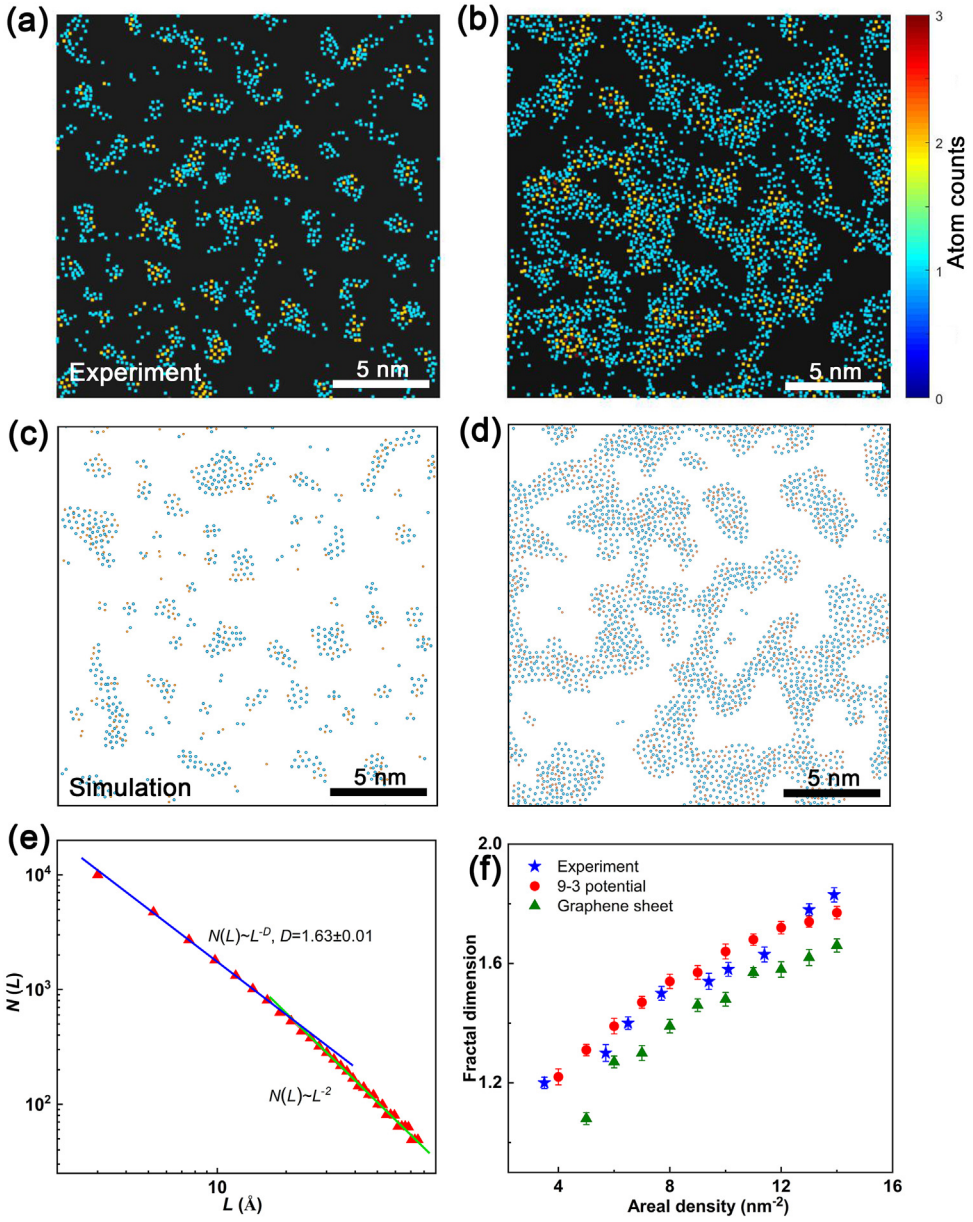


**Fig. 2.** (Color online) The fractal analysis of the MG membranes. The refined models of experimental atomic structures with the areal densities of (a) 3.2 and (b) 11.3 $nm^{-2}$, respectively. The color represents the number of atoms per column. The simulated atomic structures (c) and (d) on 9–3 potential substrate with the areal density corresponding to these of (a) and (b). (e) The box number $N(L)$ versus box length $L$ in the box-counting method for the MG membrane in (b). (f) The fractal dimension versus the areal density for experimental and simulated MG membranes.

that the most prevalent polygons are triangles, which are commonly found in the closing packed plane of the fcc Ni or hcp Zr crystals. Meanwhile, there are also other types of polygons found in the atomic images (Fig. 3d), such as quadrangle, pentagon, and hexagon, etc., reflecting the amorphous nature of the membranes. We also made a statistical analysis on the probability distribution of bond angles for the atomic structures with different areal densities, as shown in Fig. 3e. One can see that the distribution profiles are very similar for different areal densities, and the bond angles are concentrated in the range of 45°–55° with a maximum probability peak at 52°. The distribution is in contrast with that of bulk MGs, where the peaks of probability distribution appear at ~60°, 110°, and 150° [39]. The much smoother peaks reflect a much more amorphous structure in MG membranes.

The RDF was also calculated for the MG membranes with different areal densities, as shown in Fig. 3f. One can found two peaks in the RDF curves, corresponding to the first and second neighbors in the amorphous structure. The positions for the first and second peaks in RDF are located at ~3.0 and ~5.3 Å, respectively. The first peak position (3.0 Å) is well consistent with the average atomic distance calculated based on the radius of Zr atom (1.6 Å) and Ni atom (1.3 Å) and their number ratio, suggesting the homogenous distribution of Zr and Ni atoms in the amorphous structure. By integration on the area below the RDF curve, we also obtained the coordination number of the first and second neighbors, and the variation of the coordination number with the areal density as shown in the inset of Fig. 3f. The coordination numbers of the first and second neighbors increase with the areal density. As the areal density increases from 3 to 9 $nm^{-2}$, the coordination number increases from 5 to 7 for the first neighbor and from 6 to 11 for the second neighbor. The corresponding coordinate numbers are almost half of those of 3D MGs [40].

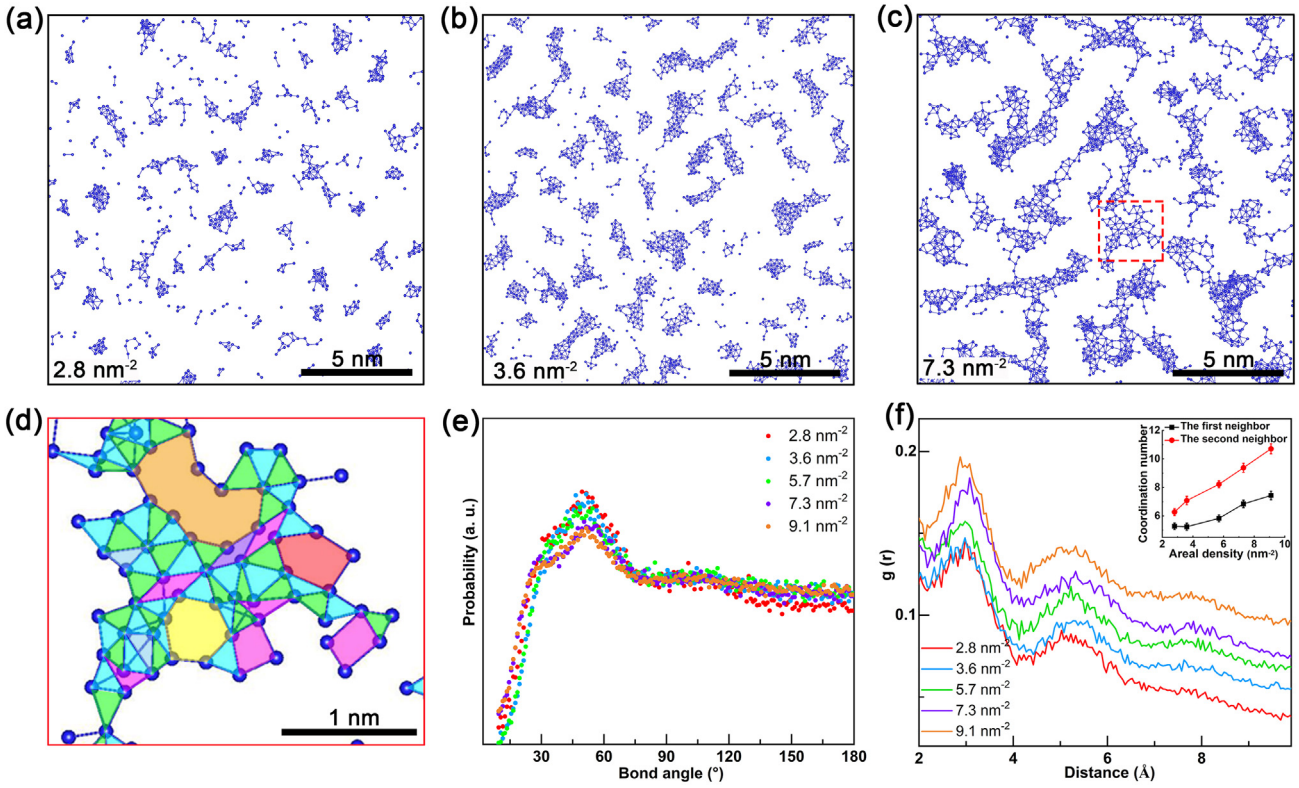


**Fig. 3.** (Color online) Analysis of atomic configuration. (a–c) The atomic configurations of $Zr_{70}Ni_{30}$ MG membranes with the areal densities of 2.8, 3.6, and 7.3 nm$^{-2}$, respectively. (d) The enlarged image of a selected region, red dotted box in (c). Color overlay is added for identification of triangles (blue and green regions), quadrangles (pink and purple regions), pentagon (red region), hexagon (yellow region), and hendecagon (orange region). (e) The distribution of bond angles and (f) the radial distribution functions for the MG membranes with the areal density. Inset in (f): the coordination number of the first (black square) and second (red circle) neighbors of MG membranes with the areal density.

The percolation theory has been used to describe the fractal structure of bulk MGs [12,41]. In the model, the system will not be connected or percolated until the probability of occupied sites $p$ reaching the percolating threshold $p_c$. A unique feature of the percolation model is the existence of the correlation length $\xi$, which characterizes the size of the finite fractal cluster at the concentration below or above $p_c$. That is to say, the system is fractal below the range of correlation length. The correlation length $\xi$ is defined as [42]

$$\xi^2 = \frac{2\Sigma R_s^2 s^2 n_s}{\Sigma s^2 n_s}, \quad (1)$$

where $R_S$, $s$, and $n_S$ are the gyration radius, number of atoms, and number of individual s-clusters, respectively. The deposition processes resemble the generation of percolation clusters in percolation theory, despite the fact that there is no explicit particle-particle interaction in percolation theory. For the deposited structures, the occupied probability $p$ is proportional to the areal density $\rho$, thus the correlation length is also expected to diverge as $\rho$ approaches $\rho_c$

$$\xi = A*|\rho - \rho_c|^{-\nu}, \quad (2)$$

where $\nu$ equals to 1.333 for the 2D system, and $A$ is a constant parameter [42].

We divided each structure with low areal density into independent percolation clusters and calculated the correlation length $\xi$ for the amorphous MG structures with different areal densities according to Eq. (1). The variation of the correlation length with the areal density is shown in Fig. 4a. One can see that the experimental correlation length can reach ~30 Å for $\rho$ = ~6 nm$^{-2}$, which is much larger than the MRO scale (~10 Å) for bulk MGs [9,10]. Even for the low areal density (~2 nm$^{-2}$), the $\xi$ extend beyond the range of MRO (~10 Å). This suggests that the fractal structure found in MGs membranes has a long-range nature. This is different from the 3D bulk MGs where the fractal structure is accused of the correlation length scale in the MRO scale and the fictitious large correlation length due to the arbitrary selection of subgroup of atoms [15]. Here, the deposition process allows for the direct modulation of the areal density and correlation length scale, thus enables the emergence of fractal in the long-range scale for MGs membranes. The dependence of correlation lengths on the areal density in MD simulations can be well fitted with Eq. (2), as shown in Fig. 4a. We note that the correlation length could also be fitted via the intersection point of two linear fittings in box-counting method. However, the overlap of excircle of individual percolation cluster may lead to the decrease of correlation length for the whole structure. The growth of the fractal structure can be well described by the percolation model, suggesting that the formation of the fractal structure is a typical critical process in MGs membranes. We can also simply connect the fractal dimensions of MG membranes and bulk MGs. As the fractal morphologies are the similar branched structures for MG membranes and bulk MGs, the fractal of 2D MGs can be converted to that of 3D MGs via the ratio of 3/2. The fractal dimension at the percolation threshold is ~1.6 for 2D MGs, thus the fractal in 3D MGs is estimated to be greater than 2.4 [12].

The fractal atomic structure found here can be related to many unique properties and behaviors in MG membranes. For example, the atomically thin glassy films or glass surfaces were reported to exhibit enhanced relaxation dynamics and a reduced glass transition temperature ($T_g$) as compared to the bulk glasses [16,17,43]. The fractal membrane structure has many atomic-scale voids or

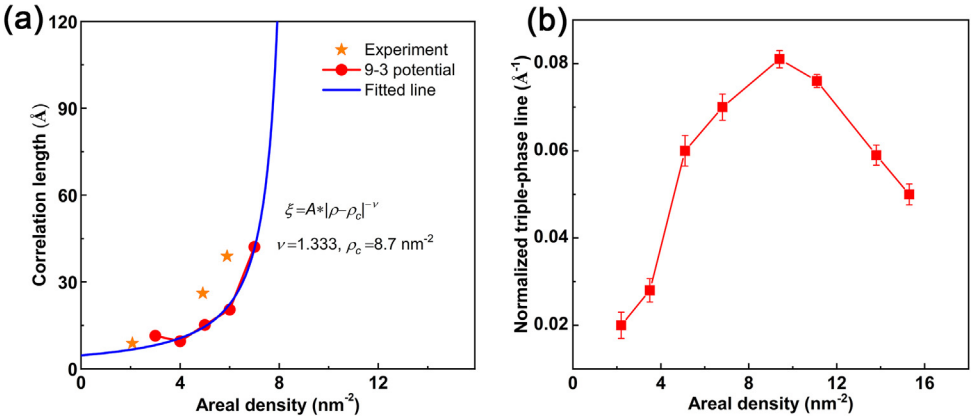


**Fig. 4.** (Color online) Percolation theory and triple-phase-line studies of the MG membranes. (a) The correlation length varies with the areal density for experimental and simulated MG membranes. The data can be fitted by the blue line and the formula is shown next to the line. (b) The length of triple-phase-line per unit area for MG membranes with the areal density.

free volume, whose sizes also follow a power-law distribution. The interconnected branching structure in fractal MG membrane also leads to the extremely long triple-phase line at the interface, i.e., the boundary length of clusters or voids. The calculated length of triple-phase line per unit area increases with the areal density, reaching the maximum of ~0.08 Å$^{-1}$ at the areal density of 9.4 nm$^{-2}$ close to the percolation threshold of 8.7 nm$^{-2}$ (Fig. 4b). The ultra-long triple-phase line can provide active sites for atomic mobility, contributing to the enhanced relaxation dynamics and the reduced $T_g$. In addition, with the further deposition, the atomic packing will undergo the transition from 2D to 3D, and intermediate states with distinctive characteristic may emerge. For example, the deposited thick MG membranes are demonstrated to exhibit enhanced thermodynamic performances [38]. However, the understanding calls for further experimental and theoretical explorations, such as tilt-series of 2D projection imaging and density functional theory calculations.

## 4. Conclusion

In summary, we directly observed the atomic arrangements in atomically thin MG membranes through the advanced HAADF-STEM technique. The global atomic packing in the amorphous structure is found to have a fractal nature, with the measured fractal dimension depending on the atomic density. The atomic configuration for the MG membranes is dominated by the triangular clusters and the bonding angles of 45°–55°. The fractal atomic structure is well described by the percolation theory. These results provide new insights for the understanding of the packing structures of MG materials and their unique relaxations and glass transition process.

## Conflict of interest

The authors declare that they have no conlfict of interest.

## Acknowledgments

This work was supported by the National Natural Science Foundation of China (51672307, 51801230, 51822107, and 51671121), the National Key Research and Development Program of China (2018YFA0703603), the National Natural Science Foundation of Guangdong Province (2019B030302010), the Strategic Priority Research Program of the Chinese Academy of Sciences (XDB30000000), and Beijing Natural Science Foundation (Z190010). We thank the fruitful discussions with Dr. Yuren Wen, Dr. Dongdong Xiao, Fanqi Meng, Xiaozhi Liu, and Tongtong Shang during the course of the study.

## Author contributions

Hongyu Jiang, Baoan Sun, and Lin Gu conceived the idea and designed the experiment. Hongyu Jiang and Qinghua Zhang carried out the experiment. Jiyu Xu performed the MD simulations with the help of Yitao Sun. Laiquan Shen and Ming Liu performed the AFM measurements. Baoan Sun, Lin Gu, and Weihua Wang directed the entire research. Hongyu Jiang, Jiyu Xu, Sheng Meng, Baoan Sun, and Lin Gu analyzed the data and wrote the manuscript. Hongyu Jiang, Jiyu Xu, Qinghua Zhang, Qian Yu, Chengrong Cao, Dong Su, Haiyang Bai, Baoan Sun, Lin Gu, and Weihua Wang contributed to the discussion of results, editing and revising the paper.

## Appendix A. Supplementary materials

Supplementary materials to this article can be found online at https://doi.org/10.1016/j.scib.2021.02.020.

## References

[1] Egami T, Poon SJ, Zhang Z, et al. Glass transition in metallic glasses: a microscopic model of topological fluctuations in the bonding network. Phys Rev B 2007;76. 024203.
[2] Johnson WL, Samwer K. A universal criterion for plastic yielding of metallic glasses with a $(T/T_g)^{2/3}$ temperature dependence. Phys Rev Lett 2005;95:195501.
[3] Angell CA. Formation of glasses from liquids and biopolymers. Science 1995;267:1924–35.
[4] Leocmach M, Tanaka H. Roles of icosahedral and crystal-like order in the hard spheres glass transition. Nat Commun 2012;3:974.
[5] Elliott SR. Physics of amorphous materials. 2nd ed. London: Longman; 1990. p. 139–51.
[6] Bernal JD. Geometry of the structure of monatomic liquids. Nature 1960;185:68–70.
[7] Gaskell PH. A new structural model for transition metal-metalloid glasses. Nature 1978;276:484–5.
[8] Gaskell PH. Amorphous metals. Singapore: World Scientific Publishing; 1985. p. 35–57.
[9] Miracle DB. A structural model for metallic glasses. Nat Mater 2004;3:697–702.
[10] Sheng HW, Luo WK, Alamgir FM, et al. Atomic packing and short-to-medium range order in metallic glasses. Nature 2006;439:419–25.
[11] Ma D, Stoica AD, Wang X-L. Power-law scaling and fractal nature of medium-range order in metallic glasses. Nat Mater 2009;8:30–4.
[12] Chen DZ, Shi CY, An Q, et al. Fractal atomic-level percolation in metallic glasses. Science 2015;349:1306–10.
[13] Zeng Q, Lin Y, Liu Y, et al. General 2.5 power law of metallic glasses. Proc Natl Acad Sci USA 2016;113:1714–8.

[14] Zhang HJ, Qiao KY, Han YL. Power laws in pressure-induced structural change of glasses. Nat Commun 2020;11:2005.
[15] Ding J, Asta M, Ritchie RO. On the question of fractal packing structure in metallic glasses. Proc Natl Acad Sci USA 2017;114:8458–63.
[16] Cao CR, Lu YM, Bai HY, et al. High surface mobility and fast surface enhanced crystallization of metallic glass. Appl Phys Lett 2015;107:141606.
[17] Zhang P, Maldonis JJ, Liu Z, et al. Spatially heterogeneous dynamics in a metallic glass forming liquid imaged by electron correlation microscopy. Nat Commun 2018;9:1129.
[18] Singh S, Ediger MD, de Pablo JJ. Ultrastable glasses from in silico vapour deposition. Nat Mater 2013;12:139–44.
[19] Yu H-B, Luo Y, Samwer K. Ultrastable metallic glass. Adv Mater 2013;25:5904–8.
[20] Xie YJ, Sohn S, Wang ML, et al. Supercluster-coupled crystal growth in metallic glass forming liquids. Nat Commun 2019;10:915.
[21] Tan Y, Zhu F, Wang H, et al. Noble-metal-free metallic glass as a highly active and stable bifunctional electrocatalyst for water splitting. Adv Mater Interfaces 2017;4:1601086.
[22] Guo H, Yan PF, Wang YB, et al. Tensile ductility and necking of metallic glass. Nat Mater 2007;6:735–9.
[23] Huang PY, Kurasch S, Alden JS, et al. Imaging atomic rearrangements in two-dimensional silica glass: watching silica's dance. Science 2013;342:224–7.
[24] Toh C-T, Zhang HJ, Lin JH, et al. Synthesis and properties of free-standing monolayer amorphous carbon. Nature 2020;577:199–203.
[25] Zhu F, Nguyen HK, Song SX, et al. Intrinsic correlation between β-relaxation and spatial heterogeneity in a metallic glass. Nat Commun 2016;7:11516.
[26] Liu YH, Fujita T, Aji DPB, et al. Structural origins of Johari-Goldstein relaxation in a metallic glass. Nat Commun 2014;5:3238.
[27] De Backer A, van den Bos KHW, Van den Broek W, et al. StatSTEM: an efficient approach for accurate and precise model-based quantification of atomic resolution electron microscopy images. Ultramicroscopy 2016;171:104–16.
[28] De Backer A, Martinez GT, Rosenauer A. Atom counting in HAADF STEM using a statistical model-based approach: methodology, possibilities, and inherent limitations. Ultramicroscopy 2013;134:23–33.
[29] Plimpton S. Fast parallel algorithms for short-range molecular dynamics. J Comput Phys 1995;117:1.
[30] Mendelev MI, Kramer MJ, Hao SG, et al. Development of interatomic potentials appropriate for simulation of liquid and glass properties of $NiZr_2$ alloy. Philos Mag 2012;92:4454.
[31] Pennycook SJ. Z-contrast STEM for materials science. Ultramicroscopy 1989;30:58–69.
[32] Findlay SD, Shibata N, Sawada H, et al. Dynamics of annular bright field imaging in scanning transmission electron microscopy. Ultramicroscopy 2010;110:903–23.
[33] Bals S, Kabius B, Haider M, et al. Annular dark field imaging in a TEM. Solid State Commun 2004;130:675–80.
[34] Liebovitch LS, Toth T. A fast algorithm to determine fractal dimensions by box counting. Phys Lett A 1989;141:386–90.
[35] Labini FS, Gabrielli A, Montuori M, et al. Finite size effects on the galaxy number counts: evidence for fractal behavior up to the deepest scale. Phys A 1996;226:195–242.
[36] Fan Y, Iwashita T, Egami T. Crossover from localized to cascade relaxations in metallic glasses. Phys Rev Lett 2015;115. 045501.
[37] Wang Z-J, Li M-X, Yu J-H, et al. Low-iridium-content irnita metallic glass films as intrinsically active catalysts for hydrogen evolution reaction. Adv Mater 2020;32:1906384.
[38] Luo P, Cao CR, Zhu F, et al. Ultrastable metallic glasses formed on cold substrates. Nat Commun 2018;9:1389.
[39] Fukunaga T. Voronoi analysis of the structure of Ni-Zr-Al ternary metallic glass. Mater Trans 2007;48:1698–702.
[40] Yang L. Atomic structure in $Zr_{70}Ni_{30}$ metallic glass. J Appl Phys 2007;102:083512.
[41] Yang MH, Li JH, Liu BX. The fractal correlation between relaxation dynamics and atomic-level structures observed in metallic glasses by computer simulation. Phys Chem Chem Phys 2017;19:16850–6.
[42] Stauffer D, Aharnoy A. Introduction to percolation theory. London: Taylor & Francis; 1994.
[43] Ellison CJ, Torkelson JM. The distribution of glass-transition temperatures in nanoscopically confined glass formers. Nat Mater 2007;2:695–700.

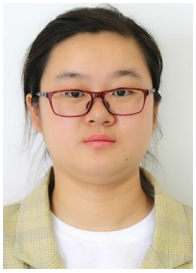

Hongyu Jiang is a postdoctoral fellow at the Institute of Physics, Chinese Academy of Sciences (IOP-CAS). She earned her Ph.D. degree in Condensed Matter Physics at IOP-CAS in 2019. Her research interest includes structural characteristics, functional applications and relaxation dynamics in low-dimensional amorphous alloys. She currently focuses on researching the atomic-level structural features of low-dimensional amorphous alloys with the advanced electronic microscope techniques.

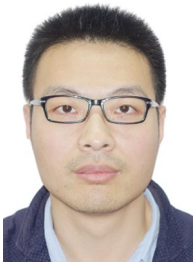

Baoan Sun is an associate professor at IOP-CAS. He received his Ph.D. degree at IOP-CAS in 2011, and then moved to Leibniz Institute for Solid State and Materials Research and City University of Hong Kong as postdoctoral fellow from 2011 to 2016. He was youth professor at Nanjing University of Science and Technology from 2016 to 2018. His research interest is mainly focused on the mechanical behavior from the micro/nano- to the mm scale, including their plastic flow and fracture and the atomic-scale physical mechanism of amorphous solids, especially on bulk metallic glasses.

Qinghua Zhang is an associate professor at IOP-CAS. He received his Ph.D. degree at IOP-CAS in 2014, and then conducted postdoctoral research at Tsinghua University from 2014 to 2017. His main research interest focuses on the atomic scale structure of functional oxides and energy materials using spherical aberration correction electron microscopy imaging technology.

Lin Gu is a professor of the Beijing Laboratory for Electron Microscopy at IOP-CAS. He received his B.E. degree from Tsinghua University in 2002, and his Ph.D. degree in Material Science from Arizona State University, USA in 2005. Part of his current research focuses on the atomic-scale characterization of electrode materials for rechargeable batteries through aberration-corrected STEM and developing new in situ electrochemical experimental methods for advanced functional materials.